Brain hematoma computational segmentation

IOP Conf. Series: Journal of Physics: Conf. Series **1126** (2018) 012071 doi:10.1088/1742-6596/1126/1/012071

Brain hematoma computational segmentation

F Sáenz[1], M Vera[2,3], Y Huerfano[3], V Molina[4], L Martinez[4], M I Vera[5], W Salazar[5], E Gelvez[2], J Salazar[2], O Valbuena[6], H Robles[7], M Bautista[1] and J Arango[1]

[1] Facultad de Ingeniería, Universidad Simón Bolívar, San José de Cúcuta, Colombia
[2] Facultad de Ciencias Exactas y Biomédicas, Universidad Simón Bolívar, San José de Cúcuta, Colombia
[3] Grupo de Investigación en Procesamiento Computacional de Datos, Universidad de Los Andes, San Cristóbal, Venezuela
[4] Grupo de investigación GINIC-HUS, Universidad ECCI, Bogotá, Colombia
[5] Servicio de Neurología, Hospital Central, San Cristóbal, Venezuela
[6] Grupo de Investigación en Educación Matemática, Matemática y Estadística (EDUMATEST), Universidad de Pamplona, Pamplona, Colombia
[7] Universidad del Sinú-Elías Bechara Zainúm, Montería, Colombia

E-mail: m.avera@unisimonbolivar.edu.co

Abstract. In computed tomography imaging, brain hematoma (BH) segmentation is a very challenging process due to a high variability of BH morphology, low contrast and noisy images. Because of this, BH segmentation is an open problem. In order to approach this problem, we propose an automatic technique, named nonlinear technique (NLT), based on a thresholding method, noise suppression filters, intelligent operators, a clustering strategy and a binary morphological operator. NLT performance is assessed by Jaccard's similarity index (JSI) used to compare automatic and manual BH segmentations. This assessment allows developing a tuning process for establishing the optimal parameters of each of the algorithms which constitute the proposed technique. The results indicate a good correlation, based on JSI, between the manual segmentations and the automatic ones. Finally, the BH volume is generated considering the automatic segmentation. This volume indicates whether or not the patient must undergo a surgical intervention for BH treatment.

1. Introduction

Brain hematomas (BH) can be classified in several ways. For example, a very simple brain hematoma classification is presented in Figure 1 [1].

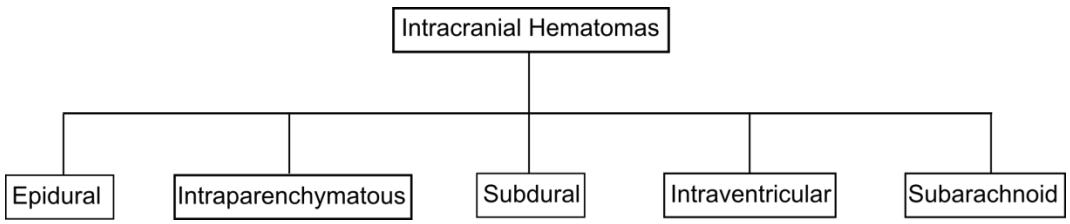

Figure 1. Block diagram for brain hematoma classification.

Additionally, the main difficulties with brain images are the Poisson noise and low contrast between the brain tissues [2].

Li-Hong and Wu [3] report lesion image detection, based on k-means segmentation, in magnetic resonance imaging (MRI). They point at a very high score linked to BH segmentation.

Roy *et al.* [4] show an automatic technique for segmentation of brain hemorrhages using thresholding method, wavelet transform, convex hull technique and gamma transform in MRI. Their results are promising since they get a good similarity index value.

An automatic technique based on convolutional neural networks [5] is reported. They apply deep learning for the BH segmentation in MSCT and MRI images and they report a mean Dice score (Ds) of 0.90.

In addition, an automatic computational technique for BH segmentation [6] is developed considering computed tomography (CT) images. This technique includes the following steps: a) maximum, mean and Gaussian filters application. b) Implementation of multi-resolution level sets to obtain the BH segmentations. An excellent Ds value, for all segmented BH, is reported.

On the other hand, this paper is an extension of the work presented in [7]. The contributions are a) Incorporation of borders detector based on a gradient filter. b) Use of Generalized Hough Transform in order to detect the coordinates of seed points. c) Precise segmentation of epidural, intraparenchymatous and subdural hematomas.

2. Materials and methods

2.1. Datasets

12 three-dimensional CT datasets were used, supplied by the Instituto de BioIngeniería y Diagnóstico S.A-Táchira-Venezuela (Bioengineering and Diagnose Institute S.A., Táchira, Venezuela). They correspond to anatomical structures present in patients with epidural (n=4), subdural (n=4) and intraparenchymatous (n=4) hematomas.

2.2. Computational strategy suggested

Figure 2 shows a scheme of the nonlinear technique (NLT) proposed in the present investigation, to segment the BH.

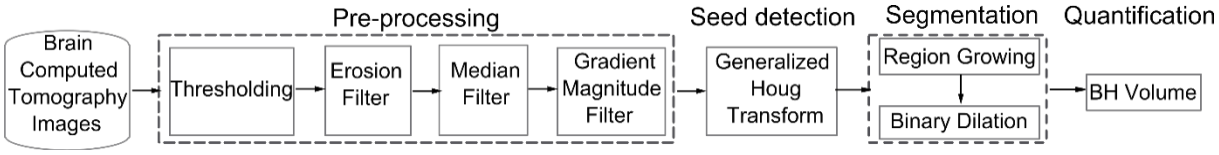

Figure 2. Scheme the proposed technique (NLT).

2.3. Filter bank

In this stage, a filter bank is applied to the datasets described in 2.1. A brief explanation of these filters is found below.

2.3.1. Histogram-thresholding method. This kind of thresholding method (TM) can use a histogram for threshold selection [8]. In this sense, the thresholds linked to BH were considered to isolate intraparenchymatous, epidural and subdural hematomas in CT datasets.

2.3.2. Morphological erosion (ME) and dilation (MD) filters. The mathematical models of morphological erosion ($\ominus$) and dilation ($\oplus$) filters, considering an image (*A)* and a structuring element (*B)*, are shown using Equations (1) and (2).

$$(A \ominus B) = \{x \,|(B)x \subset A\} \tag{1}$$

$$(A \oplus B) = \{x \,|(B)x \cap A \neq \varnothing\} \tag{2}$$

In this work, a cubic structuring element was considered, and its size is considered a parameter to control the performance of the erosion and dilation process.

2.3.3. Median Filter. The median filter is used in several applications for noise reduction. This filter is based on the median statistical concept. Usually, using an observation window with an arbitrary size, the image is scanned, resulting in a filtered image in which its edges do not fade. A more detailed description is presented in [7]. In this paper, the parameter that controls the performance of the median filter is the size of the observation window.

2.3.4. Gradient magnitude filter (GMF). The role of this filter is to detect the edges of the structures present in the images. The magnitude of the gradient, based on partial derivatives $\left(\frac{\partial I}{\partial i}, \frac{\partial I}{\partial j}, \frac{\partial I}{\partial z}\right)$, is widely used in image analysis, mainly to identify the contours of objects and the separation of homogeneous regions. Edge detection is the detection of significant discontinuities in the level of gray or color of an image [9]. The classic 3D mathematical model, to obtain a filtered image by gradient magnitude (I_{GM}), is presented by Equation (3). In this work, a scheme based on central finite differences was used for GMF computational implementation.

$$I_{GM} = \left(\left(\frac{\partial I}{\partial i}\right)^2 + \left(\frac{\partial I}{\partial j}\right)^2 + \left(\frac{\partial I}{\partial k}\right)^2\right)^{1/2} \quad (3)$$

where: *i, j, k* represents the spatial directions in which the gradient is calculated.

2.4. Segmentation

This stage involves two steps: seed point detection and region growing segmentation. An explanation of these is presented next.

2.4.1. Seed point detection. The Generalized Hough Transform (GHT) is a smart operator and it has been used to detect objects present in images using two processes. A training process, through which a parameterized reference of the object to be detected is obtained and a validation process is used for detecting the same object in unseen images during the training. In this paper, considering the I_{GM}, the GHT is used in order to detect a "seed point" for region growing initialization.

In [10], it is possible to obtain detailed information about "seed point" detection using GHT in medical images. The general scheme of GHT, taken from [10] and modified by the authors of this article, is shown in Figure 3.

In the present paper, a Labelled image (Li) is given by the $I_{GM,}$ and the "seed point" is matched to the centroid obtained when calculating the maximum argument of the accumulator (A), mentioned in Figure 3.

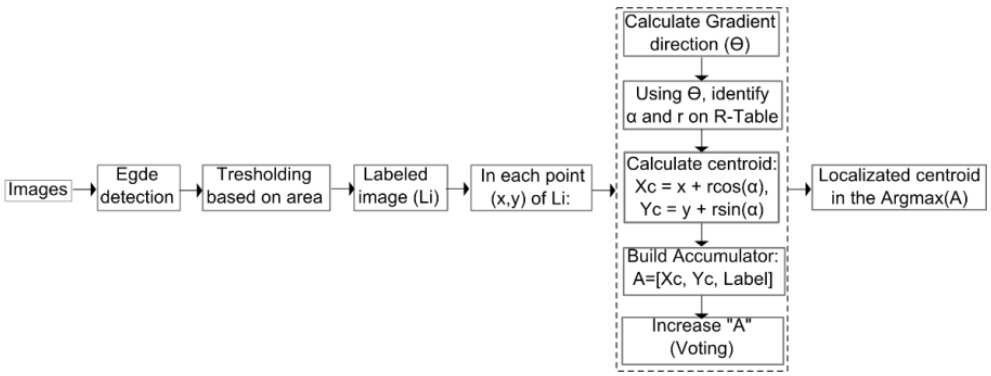

Figure 3. GHT used for "seed point" localization.

2.4.2. Region growing (RG). A detailed description of Region Growing is presented in [7]. The initial position for region growing initialization is given by seed point coordinates. The most popular criterion for including voxels in a region is defined by an intensity range around the mean value of intensities that belong to the initial neighbourhood of a seed point.

The size of this initial neighbourhood is controlled by an arbitrary radius (r). Additionally, the interval of intensities is computed as the product of the variance and an arbitrary scalar (m). Both r and m require tuning.

2.5. Tuning process

It is necessary to carry out a tuning process taking into account one of the datasets described in section 2.1. It uses an isotropic approach and considers the range of values shown in Table 1.

Table 1. Range of values of morphological and median filters.

Erosion and dilation filter	Median filter
[1,1,1], [2,2,2],…,[10,10,10], [11,11,11]	[1,1,1], [3,3,3], [5,5,5] and [7,7,7]

Additionally, in this paper, the range of values for the RG parameters is given by $0<r<10$ with a step size equal to 1 and $0<m<10$ with a step size equal to 0.1.

During the tuning process, the Jaccard's index of similarity (JIS) is used to compare automatic and manual segmentations of BH [11]. Usually, in the medical context, the JIS is considered to establish how spatially similar are manual segmentation (MS) and automatic segmentation (AS) of any anatomical structure. The expected values for the JIS are real numbers between 0 and 1. Equation (4) gives the mathematical model that defines this index.

$$\mathrm{JIS} = \frac{|\mathrm{MS} \cap \mathrm{AS}|}{|\mathrm{MS\ U\ AS}|} \tag{4}$$

The optimal values for the parameters of the RG (r and m) are matched to the experiment that generates the highest value for the JIS. This fact indirectly, allows establishing the optimal parameters for filters.

3. Results

A maximum JIS of 0.90 is obtained from the tuning process, which generated the optimal parameters for morphological filters [erosion (5,5,5) and dilation (5,5,5)] and for the region growing technique (r=6, m=3). Figure 4 shows an axial view of an original image using the selected dataset, and the images linked to digital processing developed with the proposed technique.

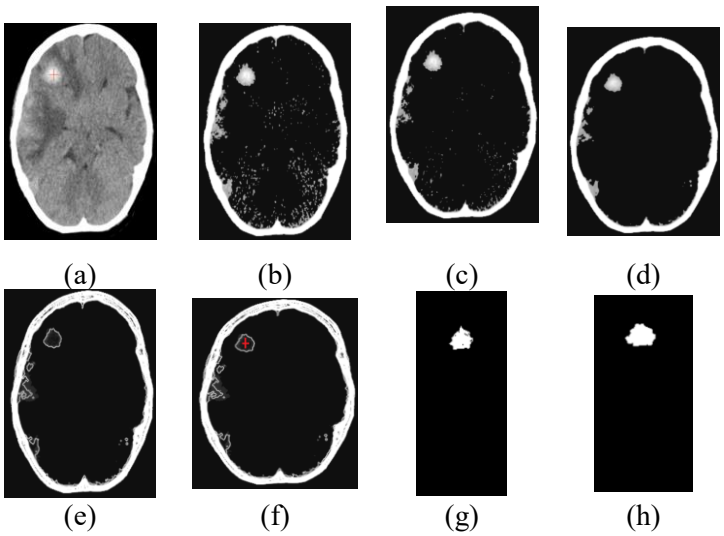

Figure 4. Effect of the NLT using a 2D view of *intraparenchymatous* hematoma. (a) original, (b) TM, (c) ME, (d) Median, (e) IGM, (f) GHT, (g) RG and (h) MD.

Additionally, Figure 5 shows the 3D morphology of segmented BH.

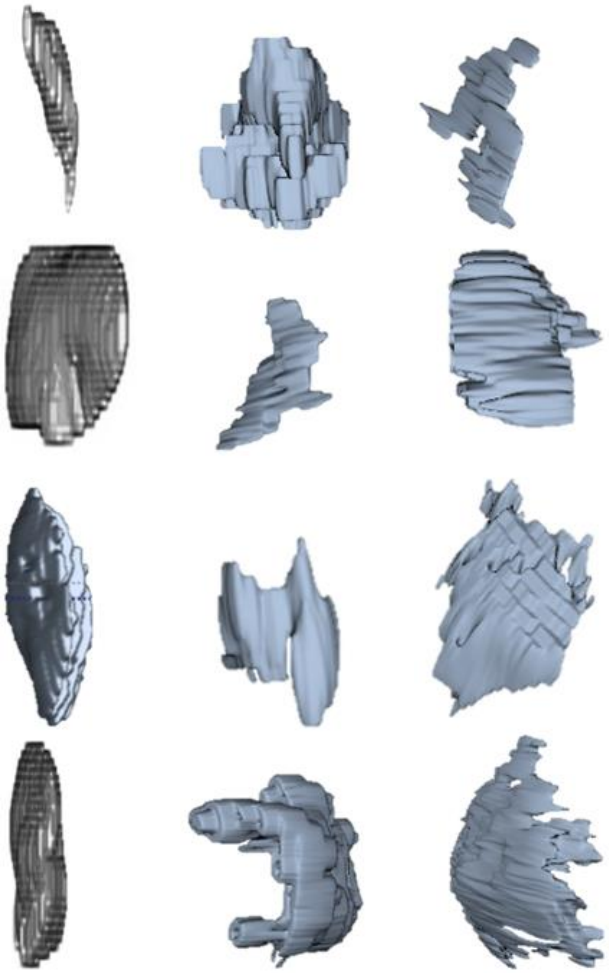

(a) (b) (c)

Figure 5. Three-dimensional representation of segmented brain hematomas. (a) Epidural, (b) Intraparenchymatous and (c) Subdural.

Finally, Table 2 shows the volume values (voxel size by the number of BH voxels) considering the automatic segmentations of the BH [12].

Table 2. Volumes associated with segmented BH.

	Volume (cm^3)			
Subdural	2.67	10.81	4.09	16.43
Intraparenchymatous	2.53	28.09	26.87	40.52
Epidural	10.89	29.77	26.49	56.22

According to the results, the maximum JIS value obtained for the BH segmentation was 0.9005. This value is comparable with JIS=0.7761 [3] and JIS=0.9444 [4]. These results indicate that the NLT has a good performance when used with BH.

On the other hand, following only the volume criterion [12], patients with intraparenchymatous and epidural hematomas, corresponding to the last column of Table 2, should go into surgery since the volume of their BH has exceeded 30cm^3.

Another interesting result is the high morphological variability of considered hematomas. This fact contradicts some of the geometric hypotheses [12], established in the clinical routine, considered by clinical experts to estimate the BH volume.

4. Conclusions

The GHT allowed the automatic identification of the "seed points" for correct RG initialization. In addition, the JIS value reported in this paper suggests that the NLT has an excellent performance. The BH automatic segmentations generated by proposed technique, allow the volume calculation of each considered hematoma, without any geometrical hypotheses. One of the most important features of NLT, in this paper, is that it allows discriminating which patients should be subjected to a surgical intervention. It is planned for the future to use this technique in the segmentation and quantification of other types of hematomas affecting the human brain, such as *subarechnoid* and *intraventricular* hematomas.

References

[1] Stippler M 2016 Craniocerebral trauma *Bradley's Neurology in Clinical Practice* vol 2 ed Robert B. Daroff, Joseph Jankovic, John C Mazziotta, Scott L Pomeroy (Philadelphia: Elsevier) chapter 62 pp 867–880

[2] Maier A, Wigstrom L, Hofmann H G, Hornegger J, Zhu L, Strobel N and Fahrig R 2011 Three-dimensional anisotropic adaptive filtering of projection data for noise reduction in cone beam CT *Medical Physics* **38** 5896

[3] Li-Hong J and Wu M 2010 MRI brain lesion image detection based on colour converted k-means clustering segmentation *Measurement* **43** 941

[4] Roy S, Nag S, Bandyopadhyay S K, Bhattacharyya D and Kim T H 2015 Automated brain haemorrhage lesion segmentation and classification from MR image using an innovative composite method *Journal of Theoretical and Applied Information Technology* **78** 34

[5] Kamnitsas K, Lediga C, Newcombeb V, Simpsonb J, Kaneb A, Menonb D, Rueckerta D, Glockera B 2017 Efficient multi-scale 3D CNN with fully connected CRF for accurate brain lesion segmentation. *Med. Image Anal* **23** 1603

[6] Liao C, Xiao F, Wong J, Chiang I 2010 Computer-aided diagnosis of intracranial hematoma with brain deformation on computed tomography. *Comput Med Imaging Graph* **34** 563

[7] Vera M, Martinez L J, Huerfano Y, Molina V, Vargas S, Vera M, Salazar W, Rodriguez J, Rodriguez R, Chacon G, Isaza A, Saenz F, Glevez E and Salazar J 2018 Automatic segmentation of subdural hematomas using a computational technique based on smart operators *Global Medical Engineering Physics Exchanges/Pan American Health Care Exchanges (Porto)* **1** 1

[8] Sharma B and Venugopalan K 2012 Automatic segmentation of brain ct scan image to identify hemorrhages. *International Journal of Computer Applications* **40** 1

[9] Al-Ayyoub M, Alawad D, Al-Darabsah K and Aljarrah I 2013. Automatic detection and classification of brain hemorrhages. *WSEAS Transactions on Computers* **10** 395

[10] Vera M, Bravo A and Medina R 2011 Improving ventricle detection in 3D cardiac multislice computerized tomography images *Communications in Computer and Information Science* **229** 170

[11] Real R and Vargas J 1996. The probabilistic basis of Jaccard's index of similarity *Syst. Biol* **45** 380

[12] Hu T, Yan L, Yan P, Wang X and Yue G 2016 Assessment of the ABC/2 method of epidural hematoma volume measurement as compared to computer-assisted planimetric analysis *Biological Research for Nursing* **18** 5